

Ultrasonic-assisted hydrothermal synthesis of nanoscale double ceric phosphates

Taisiya O. Kozlova^{1,a}, Ekaterina D. Sheichenko^{1,2,b}, Darya N. Vasilyeva^{1,2,c}, Daniil A. Kozlov^{1,d}, Irina V. Kolesnik^{1,3,e}, Ilya V. Tronev^{1,2,f}, Maria A. Teplonogova^{1,g}, Alexander E. Baranchikov^{1,h}, Vladimir K. Ivanov^{1,i}

¹Kurnakov Institute of General and Inorganic Chemistry of the Russian Academy of Sciences, Moscow, Russia

²National Research University Higher School of Economics, Moscow, Russia

³Lomonosov Moscow State University, Moscow, Russia

^ataisia.shekunova@yandex.ru, ^bkseterina@yandex.ru, ^cdnavasileva_1@edu.hse.ru,

^dkozlov@inorg.chem.msu.ru, ^ekolesnik.iv@gmail.com, ^fivtronev@edu.hse.ru, ^gm.teplonogova@gmail.com,

^ha.baranchikov@yandex.ru, ⁱvan@igic.ras.ru

Corresponding author: Taisiya O. Kozlova, taisia.shekunova@yandex.ru

PACS 61.66.Fn, 43.35.Zc, 78.20.-e

ABSTRACT The combination of ultrasonic exposure on ceric phosphate gels with subsequent hydrothermal-microwave treatment resulted in the formation of nanoscale $\text{NH}_4\text{Ce}_2(\text{PO}_4)_3$ or $\text{KCe}_2(\text{PO}_4)_3$ phases. The sun protection factor (SPF) and protection factor against UV-A radiation (UVAPF) values for double ceric phosphates with the smallest crystallite sizes exceeded 4 and 3.5, respectively, which is much higher than the values for samples consisting of larger particles. These results are superior to previously published values for similar ceric compounds, and thus show promise for their application in sunscreens.

KEYWORDS cerium, ultrasonic exposure, microwave, particle size, UV shielding

ACKNOWLEDGEMENTS This work was supported by Russian Science Foundation (Grant no. 23-73-10088, <https://rscf.ru/en/project/23-73-10088/>) using the equipment of the JRC PMR IGIC RAS.

FOR CITATION Kozlova T.O., Sheichenko E.D., Vasilyeva D.N., Kozlov D.A., Kolesnik I.V., Tronev I.V., Teplonogova M.A., Baranchikov A.E., Ivanov V.K. Ultrasonic-assisted hydrothermal synthesis of nanoscale double ceric phosphates. *Nanosystems: Phys. Chem. Math.*, 2024, **15** (2), 215–223.

1. Introduction

Modern sunscreens are cosmetic preparations containing organic or inorganic UV filters as active ingredients. The use of organic UV filters in sunscreens is less preferred due to their potential to penetrate the skin barrier and to exhibit systemic effects in the body, their relatively low photostability, and ability to generate reactive oxygen species under irradiation [1, 2]. The latter drawback is also characteristic of commercial metal oxide UV filters, such as TiO_2 or ZnO [3–5]. Phosphate compounds are considered as alternative inorganic UV filters because of their biocompatibility, high chemical and thermal stability of the phosphate matrix [6–8]. Recently, crystalline cerium(IV) phosphates were reported to be promising sunscreen candidates [9–12]. The primary method for synthesizing these compounds is through hydrothermal treatment, which typically results in the formation of micron or submicron particles [13–19]. However, the size of the inorganic components is a crucial parameter that can impact photoprotective properties, distribution uniformity over the skin, and overall appearance of cosmetic compositions [20–22]. In this regard, an important task is to develop methods for producing inorganic UV filter particles with a specific mean particle size and narrow size distribution. Previously, we demonstrated the use of the hydrothermal-microwave method, instead of conventional hydrothermal treatment, to produce particles of ammonium-cerium(IV) phosphates ($\text{NH}_4\text{Ce}_2(\text{PO}_4)_3$, $(\text{NH}_4)_2\text{Ce}(\text{PO}_4)_2 \cdot \text{H}_2\text{O}$) in a wide size range by varying the duration of synthesis and temperature [23]. It is also well known that ultrasonic treatment of the reaction mixtures can reduce the particle size of products and promote their uniform distribution [24–26]. At the same time, the number of papers is still limited which report on the influence of ultrasonic pre-treatment of heterogeneous precursors, such as gels, on the products of hydrothermal synthesis.

This study investigates the effect of ultrasonication of ceric phosphate gels on their crystallization upon hydrothermal or hydrothermal-microwave treatment, resulting in the formation of $\text{NH}_4\text{Ce}_2(\text{PO}_4)_3$ or $\text{KCe}_2(\text{PO}_4)_3$ samples. The influence of mean particle size and particle size distribution of the resulting samples on their UV shielding properties is also studied.

© Kozlova T.O., Sheichenko E.D., Vasilyeva D.N., Kozlov D.A., Kolesnik I.V., Tronev I.V., Teplonogova M.A., Baranchikov A.E., Ivanov V.K., 2024

2. Experimental section

The following materials were used as received, without further purification: $\text{Ce}(\text{NO}_3)_3 \cdot 6\text{H}_2\text{O}$ (pure grade, Lanhit Russia), potassium hydroxide (pure grade, Sigma Aldrich), phosphoric acid (85 wt.% aq, $\rho = 1.689 \text{ g/cm}^3$, extra-pure grade, Komponent-Reaktiv Russia), aqueous ammonia (25 wt.%, extra-pure grade, Khimmed Russia), isopropanol (extra-pure grade, Khimmed Russia), glycerol (Sigma-Aldrich, 99.5 %), sodium dodecyl sulfate (99 %, Sigma-Aldrich), distilled water.

First, ceric phosphate solution was synthesized according to the procedure reported earlier [27]. Briefly, nanocrystalline (4 – 5 nm) cerium dioxide (0.100 g) obtained by precipitation from $\text{Ce}(\text{NO}_3)_3 \cdot 6\text{H}_2\text{O}$ aqueous solution [28] was dissolved in concentrated phosphoric acid (5 ml) at 80°C . The calculated molar ratio of Ce:P in the solution was 1:126. The cooled solution was placed into an ultrasonic bath Bandelin Sonorex Longlife RK 1050 for 30 min, then 35 ml of 0.5 M aqueous ammonia solution or 1 M potassium hydroxide aqueous solution was added to the reaction mixture. The obtained gels ($\sim 40 \text{ mL}$) were sonicated using Bandelin Sonopuls HD 3200 homogenizer operated at 20 kHz (200 W, amplitude 20 %) and equipped with titanium horn (TT-13 titanium tip) for 1 h. The resulting suspensions were placed in 100 ml Teflon autoclaves and treated under hydrothermal or hydrothermal-microwave conditions at 180°C for 24 h or 1 h, respectively. After cooling the autoclaves, the precipitates were repeatedly washed using distilled water and dried at 60°C in air. The synthesis scheme is shown in Fig. 1.

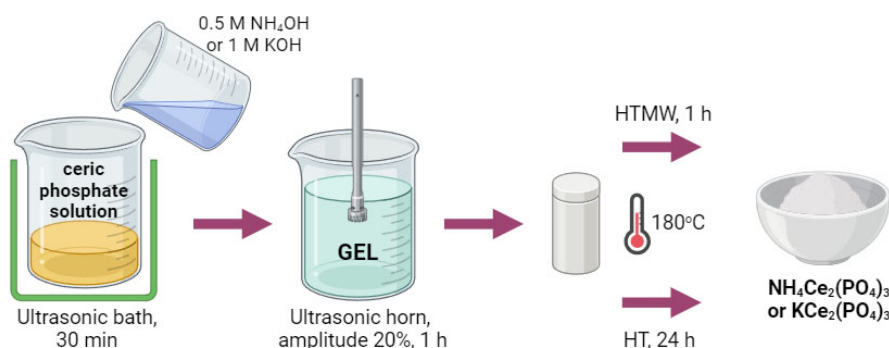


FIG. 1. The scheme of double ceric phosphates synthesis using ultrasonic-assisted hydrothermal-microwave (HTMW) or conventional hydrothermal (HT) treatment

As a reference, $\text{NH}_4\text{Ce}_2(\text{PO}_4)_3$ and $\text{KCe}_2(\text{PO}_4)_3$ samples, previously synthesized under hydrothermal conditions without the use of microwave or ultrasonic treatment [19, 23], have been obtained. These samples were designated as NCeP and KCeP, respectively.

Powder X-ray diffraction (PXRD) patterns were acquired with a DX-2700BH (Haoyuan, China) diffractometer, using $\text{Cu K}\alpha_{1,2}$ radiation in the 2θ range of $5^\circ - 80^\circ$ with 0.02° 2θ steps and a counting time of no less than 1 s per step. The identification of the diffraction peaks was carried out using the ICDD database. The full-profile analysis of diffraction patterns with quantitative determination of the coherent scattering domains (CSD) sizes, was performed using the Rietveld method realized in the MAUD software (version 2.99).

Scanning electron microscopy (SEM) images were obtained using an Amber GMH (Tescan, Czech Republic) microscope operated at an accelerating voltage of 5 kV using a secondary electron (Everhart–Thornley) detector. Particle size analysis was carried out using the ImageJ software (version 1.53t). For each sample, the sizes of at least 150 particles were measured, after which the particle size distributions were approximated by a lognormal function. Energy-dispersive X-ray spectroscopy (EDX) was performed using an Ultim Max (Oxford Instruments, UK) detector at an accelerating voltage of 20 kV.

Fourier transform infrared (FTIR) spectra of the samples were recorded using an InfraLUM FT-08 (Lumex, Russia) spectrometer in the range of $400 - 4000 \text{ cm}^{-1}$ in attenuated total reflectance mode.

Absorption spectra of $\text{NH}_4\text{Ce}_2(\text{PO}_4)_3$ and $\text{KCe}_2(\text{PO}_4)_3$ samples for band gap (E_g) determination were acquired in a diffuse reflection mode on a Lambda 950 (PerkinElmer, USA) spectrometer in the 200 – 1000 nm range. The sun protection factor (SPF) and protection factor against UV-A radiation (UVAPF) values were determined in accordance with the ISO 24443-2016, the measurement procedure and calculation formulas have previously been reported [12]. For this study, suspensions containing 10 wt.% of double ceric phosphates and 90 wt.% of a solution consisting of 9.9 wt.% H_2O , 90 wt.% glycerol and 0.1 wt.% sodium dodecyl sulfate were prepared in an agate mortar. Then, 0.035 g of each suspension was evenly spread over the surface of the 3M Transpore Tape 1527-2 film (27.5 cm^2 area). The total transmittance spectra of the films coated with the suspensions were recorded in the range of 290 – 400 nm on a Lambda 950 (PerkinElmer, USA) spectrometer using an integrating sphere (150 mm diameter). 3M Transpore Tape 1527-2 coated with a similar formulation without adding double ceric phosphates, was used as a reference sample.

3. Results and discussion

According to the PXRD data, after the hydrothermal treatment of the reaction mixtures obtained by mixing ceric phosphate solutions with a 0.5 M NH_4OH aqueous solution, $\text{NH}_4\text{Ce}_2(\text{PO}_4)_3$ phase formed (Fig. 2a). Note, that in case of hydrothermal treatment (24 h) of sonicated ceric phosphate gel an admixture of CePO_4 with monazite structure (PDF2 [00-032-199]) was detected in the sample. The presence of Ce(III) phosphate admixture in the products of hydrothermal treatment of ceric phosphate gels has been repeatedly reported [16, 19, 29, 30], what may be due to Ce(IV) reduction under specific synthesis conditions. Using the 1 M KOH aqueous solution as a precursor led to the single phase $\text{KCe}_2(\text{PO}_4)_3$ formation in all the cases (Fig. 2b). The unit cell parameters refinement as well as CSD evaluation were performed using Rietveld analysis of the PXRD patterns for $\text{NH}_4\text{Ce}_2(\text{PO}_4)_3$ and $\text{KCe}_2(\text{PO}_4)_3$ phases (Table 1). The obtained results agree well with previously published data and confirm that these double ceric phosphates are isostructural to each other [17, 19].

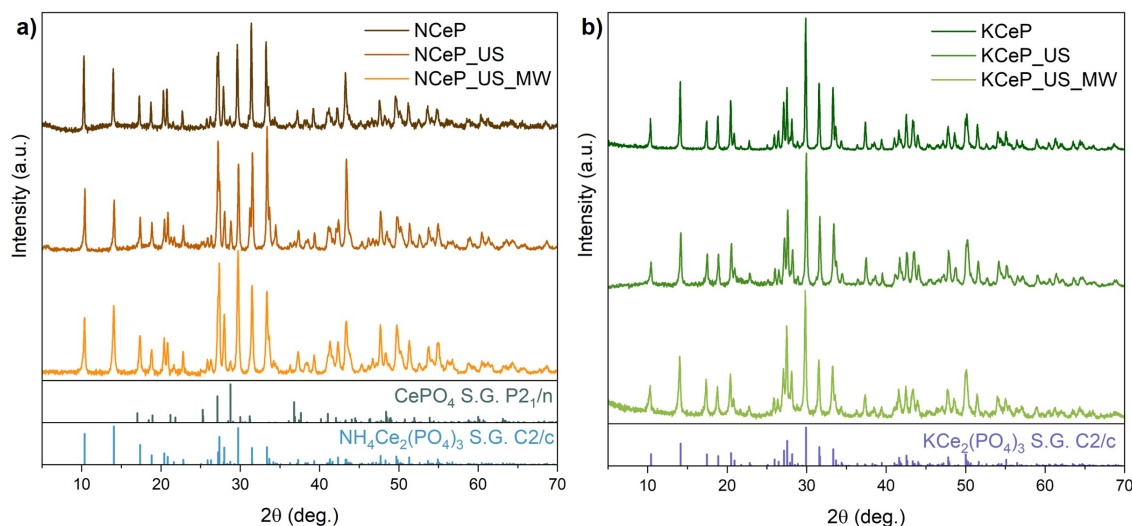


FIG. 2. Powder X-ray diffraction patterns of the products of HTMW or HT treatment of ceric phosphate gels formed upon the addition of 0.5 M NH_4OH (a) or 1 M KOH (b) to ceric phosphate solutions. The corresponding Bragg peak positions are shown below

Based on the X-ray diffraction analysis results, it was found that the use of hydrothermal-microwave treatment in comparison with conventional hydrothermal synthesis resulted in decreasing of $\text{NH}_4\text{Ce}_2(\text{PO}_4)_3$ and $\text{KCe}_2(\text{PO}_4)_3$ particle sizes. This is consistent with the findings of Tronev et al. [23], indicating the same dependence. Moreover, the same trend is observed when comparing samples obtained with or without ultrasonic pre-treatment (Table 1). Thus, the phases $\text{NH}_4\text{Ce}_2(\text{PO}_4)_3$ and $\text{KCe}_2(\text{PO}_4)_3$ with the least crystallite sizes of 60 and 65 nm, respectively, were obtained by combining microwave and ultrasonic treatment of the reaction mixtures.

IR spectroscopy data (Fig. 3) confirm the results of the PXRD analysis, indicating that the type of hydrothermal treatment and ultrasonic pre-treatment virtually has no influence on the structure of the samples. The general appearance of the IR spectra of the samples obtained is almost the same and agree well with the previously reported data for $\text{NH}_4\text{Ce}_2(\text{PO}_4)_3$ and $\text{KCe}_2(\text{PO}_4)_3$ phases [17, 19]. In the regions of $1100 - 900$ and $650 - 440 \text{ cm}^{-1}$ the absorption bands are observed, which are related to the stretching and bending vibrations of the phosphate anions, respectively [31, 32]. Furthermore, the IR spectra of $\text{NH}_4\text{Ce}_2(\text{PO}_4)_3$ samples exhibit absorption bands at $2800 - 3300 \text{ cm}^{-1}$ (broad) and 1425 cm^{-1} (sharp), which correspond to the vibrations of the NH_4^+ ion [33–35].

The particle size dependence on the synthetic method used, as observed through X-ray diffraction analysis, is clearly demonstrated in the scanning electron microscopy images (Fig. 4). Table 2 presents the mean particle sizes and standard deviations obtained from lognormal distribution as determined from scanning electron microscopy data. The mean particle sizes of $\text{KCe}_2(\text{PO}_4)_3$ samples appear to be similar to the crystallite sizes determined from XRD data. The overestimation of the corresponding values for $\text{NH}_4\text{Ce}_2(\text{PO}_4)_3$ samples is explained by the anisotropic microstructure of this phase, for which the length of single crystallites from SEM images was measured. Note that the most uniform particle size distribution is achieved through the combination of microwave and ultrasonic effects (Fig. 5).

TABLE 1. Structural parameters and crystallite sizes for the products of HTMW or HT treatment of ceric phosphate gels formed upon the addition of 0.5 M NH_4OH or 1 M KOH to ceric phosphate solutions

Sample	NCeP	NCeP_US	NCeP_US_MW	KCeP	KCeP_US	KCeP_US_MW
Precipitating agent	NH_4OH	NH_4OH	NH_4OH	KOH	KOH	KOH
Ultrasonic treatment	-	+	+	-	+	+
Type of hydrothermal treatment	HT	HT	HTMW	HT	HT	HTMW
Duration of hydrothermal treatment, h	24	24	1	24	24	1
Phase composition	$\text{NH}_4\text{Ce}_2(\text{PO}_4)_3$	$\text{NH}_4\text{Ce}_2(\text{PO}_4)_3$: 89.0±1.0 wt.% CePO_4 : 11.0±0.5 wt.%	$\text{NH}_4\text{Ce}_2(\text{PO}_4)_3$	$\text{KCe}_2(\text{PO}_4)_3$	$\text{KCe}_2(\text{PO}_4)_3$	$\text{KCe}_2(\text{PO}_4)_3$
Lattice parameters	$a = 17.491(1) \text{ \AA}$ $b = 6.7751(5) \text{ \AA}$ $c = 8.0051(6) \text{ \AA}$ $\beta = 102.868(3)^\circ$	$\text{NH}_4\text{Ce}_2(\text{PO}_4)_3$: $a = 17.4691(9) \text{ \AA}$ $b = 6.7672(4) \text{ \AA}$ $c = 8.0011(4) \text{ \AA}$ $\beta = 102.802(3)^\circ$ CePO_4 : $a = 6.799(4) \text{ \AA}$ $b = 7.016(1) \text{ \AA}$ $c = 6.4675(9) \text{ \AA}$ $\beta = 103.67(4)^\circ$	$a = 17.4804(8) \text{ \AA}$ $b = 6.7711(3) \text{ \AA}$ $c = 8.0001(4) \text{ \AA}$ $\beta = 102.836(3)^\circ$	$a = 17.373(1) \text{ \AA}$ $b = 6.7272(6) \text{ \AA}$ $b = 7.9687(6) \text{ \AA}$ $\beta = 102.350(3)^\circ$	$a = 17.372(1) \text{ \AA}$ $b = 6.7299(4) \text{ \AA}$ $c = 7.9693(5) \text{ \AA}$ $\beta = 102.351(4)^\circ$	$a = 17.376(1) \text{ \AA}$ $b = 6.7315(5) \text{ \AA}$ $c = 7.9701(6) \text{ \AA}$ $\beta = 102.306(5)^\circ$
Crystallite size, nm	> 100	> 100 CePO_4 : 72±2	60±2	> 100	75±3	65±2

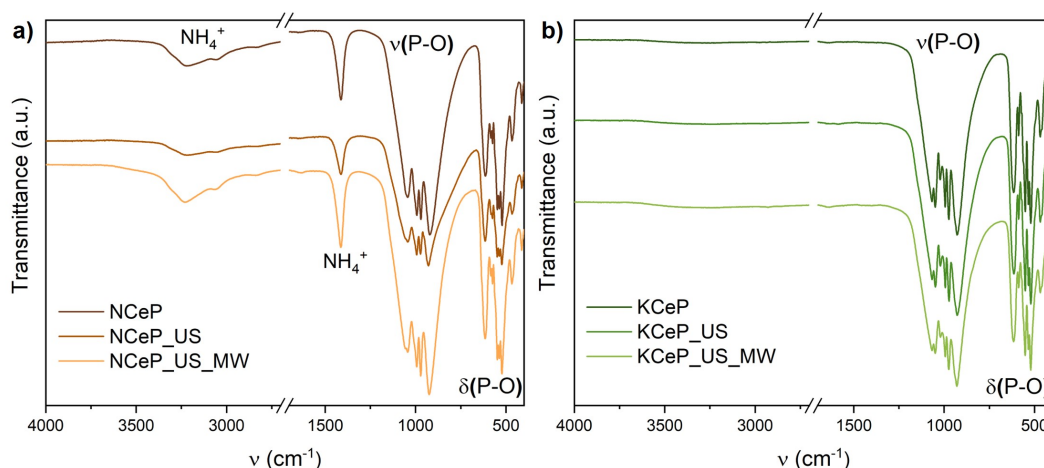


FIG. 3. IR spectra for products of HTMW or HT treatment of ceric phosphate gels formed upon the addition of 0.5 M NH_4OH (a) or 1 M KOH (b) to ceric phosphate solutions

Based on the obtained data, the ultrasonic treatment significantly affects the crystallization of double ceric phosphates under hydrothermal conditions. This observation is in line with the results of the previous studies, devoted to other inorganic systems (see e.g. [36–38]). In particular, on the example of mixed oxide particles [39] and silicoaluminophosphate molecular sieves [40] it was shown that preliminary ultrasonication inhibits the crystallite growth and leads to formation of smaller crystals with more uniform size distribution.

TABLE 2. The mean particle sizes and standard deviation determined from the SEM images for $\text{NH}_4\text{Ce}_2(\text{PO}_4)_3$ and $\text{KCe}_2(\text{PO}_4)_3$ samples

Sample	NCEP	NCEP_US	NCEP_US_MW	KCEP	KCEP_US	KCEP_US_MW
Mean particle size, nm	275	352	244	138	105	58
Standard deviation, nm	114	217	63	39	20	11

The UV-vis absorption spectra of $\text{NH}_4\text{Ce}_2(\text{PO}_4)_3$ and $\text{KCe}_2(\text{PO}_4)_3$ samples are almost identical within each series. To determine the optical band gap, optical absorption spectra were rebuilt using Tauc plot for allowed indirect transition (Fig. 6). The estimated E_g values of $\text{NH}_4\text{Ce}_2(\text{PO}_4)_3$ (2.57 – 2.61 eV) samples coincide with the previously published data [12, 23]. The corresponding values for $\text{KCe}_2(\text{PO}_4)_3$ samples (2.63 eV) were determined for the first time and are close to those of $\text{NH}_4\text{Ce}_2(\text{PO}_4)_3$.

The SPF and UVAPF values obtained in accordance with the ISO 24443-2016 international standard are shown in the Table 3. Note that the absolute values for the NCEP sample are lower than those for the $\text{NH}_4\text{Ce}_2(\text{PO}_4)_3$ sample, obtained earlier under similar conditions (SPF=2.7, UVAPF=2.5) [12]. However, even when considering the values presented in the previous work, the NCEP_US_MW sample has the highest SPF and UVAPF values. The samples produced using both ultrasonic and microwave treatment exhibit the highest UV protection properties. It is noteworthy that SPF and UVAPF values for NCEP_US_MW and KCEP_US_MW samples are higher than previously reported corresponding values for other ceric phosphates and even nanocrystalline cerium dioxide [12, 41].

TABLE 3. Sun protection factor and UVAPF protection factor values for $\text{NH}_4\text{Ce}_2(\text{PO}_4)_3$ and $\text{KCe}_2(\text{PO}_4)_3$ samples

Sample	NCEP	NCEP_US_MW	KCEP	KCEP_US_MW
SPF	1.9±0.1	4.0±0.2	3.3±0.3	3.9±0.4
UVAPF	1.9±0.1	3.9±0.3	3.5±0.5	3.5±0.4

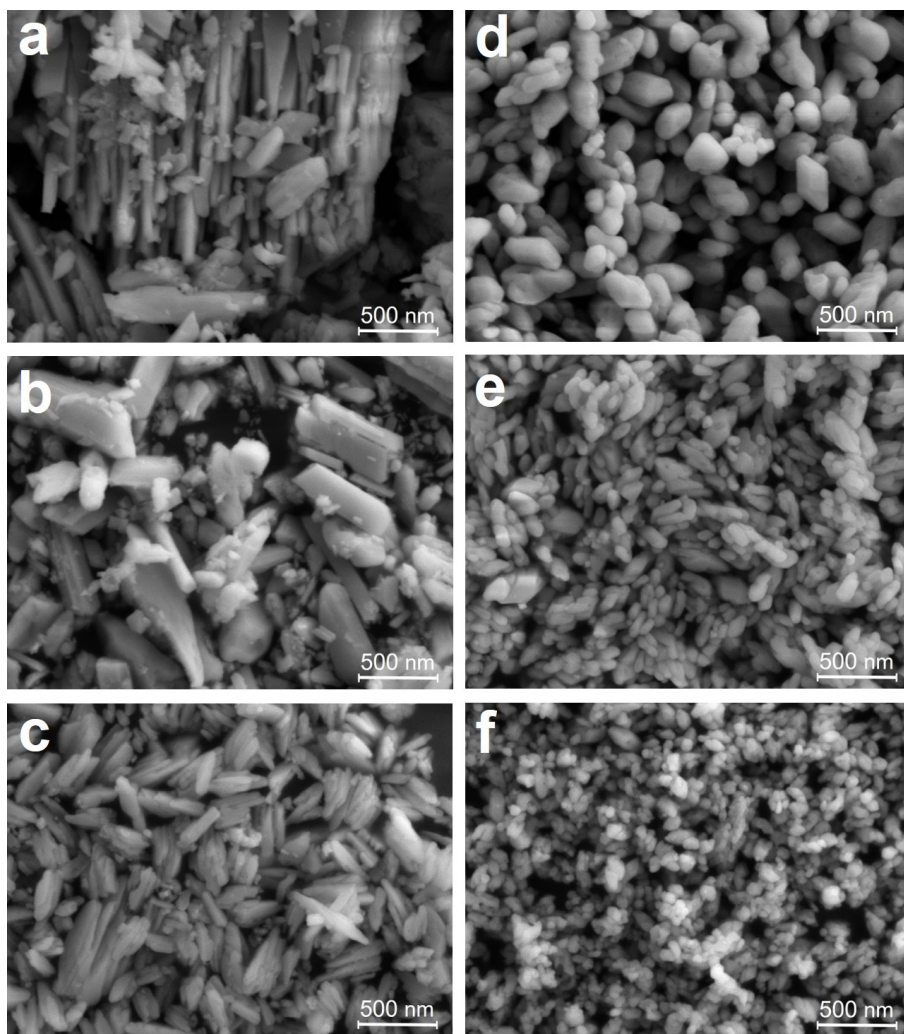


FIG. 4. SEM images of a) NCeP, b) NCeP_US, c) NCeP_US_MW, d) KCeP, e) KCeP_US, f) KCeP_US_MW samples

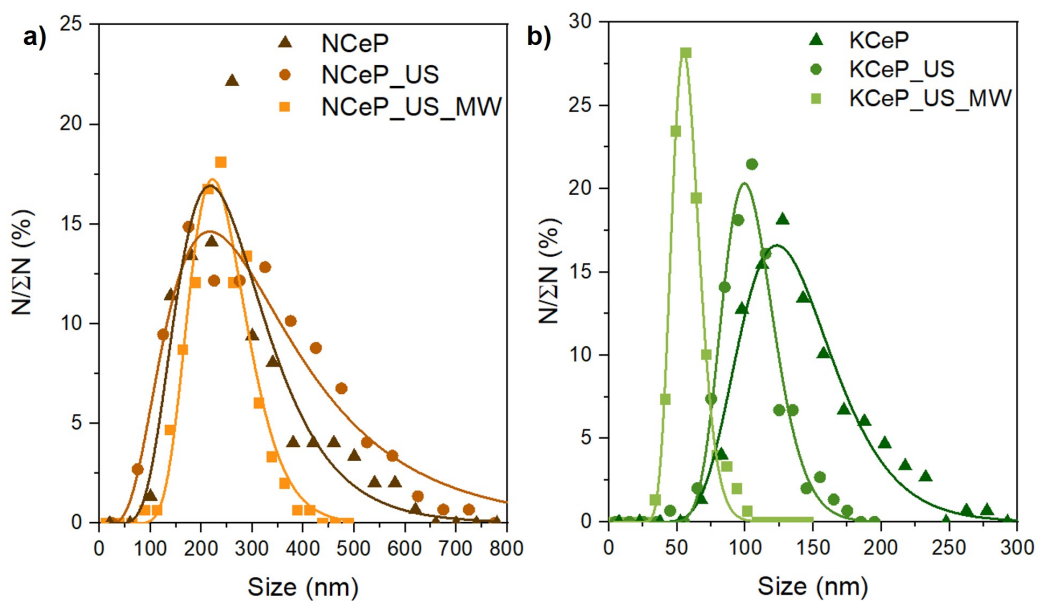


FIG. 5. Size distribution of the particles of $\text{NH}_4\text{Ce}_2(\text{PO}_4)_3$ and $\text{KCe}_2(\text{PO}_4)_3$ samples calculated from SEM data. Solid lines correspond to the results of data fitting using a lognormal distribution function

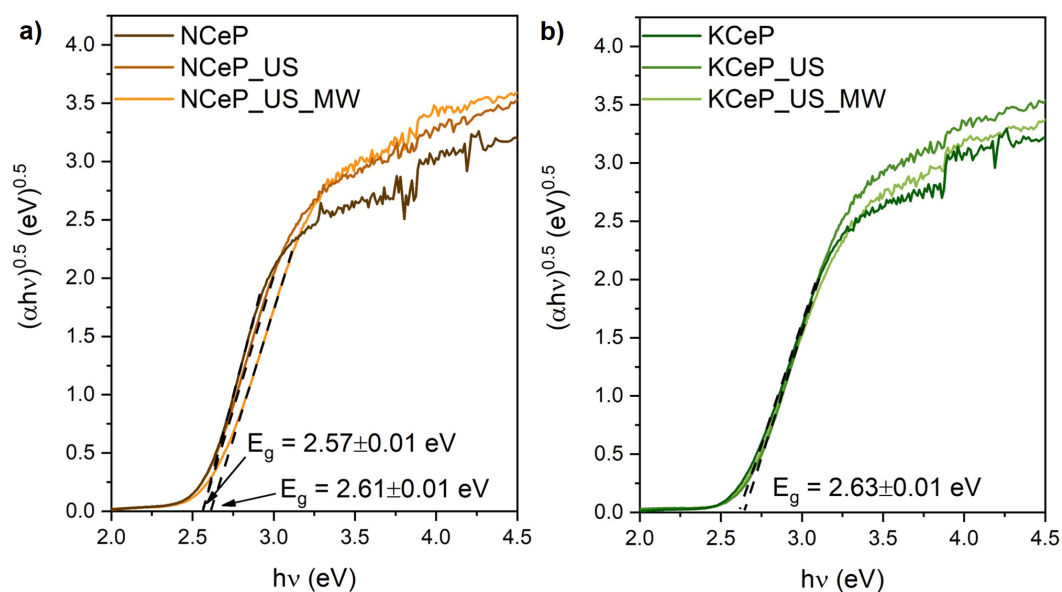


FIG. 6. Plots for band gap energy (indirect transition) determination for $\text{NH}_4\text{Ce}_2(\text{PO}_4)_3$ (a) and $\text{KCe}_2(\text{PO}_4)_3$ (b) samples

Taking into account that the optical absorption spectra of $\text{NH}_4\text{Ce}_2(\text{PO}_4)_3$ and $\text{KCe}_2(\text{PO}_4)_3$ samples are similar within each series, the increase in SPF and UVAPF values is likely due to the particle size decrease. Note, that some previous studies [42–45] also have stated the impact of inorganic filler size on the sunscreens UV shielding effect. Smaller particles contribute to a denser film formation that likely caused larger absorption in the UV region.

4. Conclusions

The study investigated the particle size distributions and UV radiation protective effects of isostructural $\text{NH}_4\text{Ce}_2(\text{PO}_4)_3$ and $\text{KCe}_2(\text{PO}_4)_3$ phases synthesized through hydrothermal and hydrothermal microwave methods, including those combined with ultrasonic pre-treatment. It has been demonstrated that the sonication of starting ceric phosphate gels followed by hydrothermal-microwave treatment allows for the production of double ceric phosphates with the smallest crystallite sizes (approximately 60 nm) and the narrowest particle size distribution. For the first time, it has been shown that the crystallite sizes of $\text{NH}_4\text{Ce}_2(\text{PO}_4)_3$ and $\text{KCe}_2(\text{PO}_4)_3$ affect their UV shielding properties. The study revealed that the sun protection factor and protection factor against UV-A radiation increase as the mean particle size of the materials decreases. The SPF and UVAPF values obtained (up to 4) are significantly higher than previously published values for similar ceric compounds.

References

- [1] Gallagher R.P., Lee T.K. Adverse Effects of Ultraviolet Radiation: A Brief Review. *Prog. Biophys. Mol. Biol.*, 2006, **92**, P. 119–131.
- [2] González S., Fernández-Lorente M., Gilaberte-Calzada Y. The Latest on Skin Photoprotection. *Clin. Dermatol.*, 2008, **26**, P. 614–626.
- [3] Wang S.Q., Balagula Y., Osterwalder U. Photoprotection: A Review of the Current and Future Technologies. *Dermatol. Ther.*, 2010, **23**, P. 31–47.
- [4] Egambaram O.P., Kesavan Pillai S., Ray S.S. Materials Science Challenges in Skin UV Protection: A Review. *Photochem. Photobiol.*, 2020, **96**, P. 779–797.
- [5] Schneider S.L., Lim H.W. A Review of Inorganic UV Filters Zinc Oxide and Titanium Dioxide. *Photodermatol. Photoimmunol. Photomed.*, 2019, **35**, P. 442–446.
- [6] Onoda H., Iwashita M. Synthesis of Novel White Pigments by Shaking Cerium Compounds with Phosphoric Acid. *Emergent Mater.*, 2023, **6**, P. 1089–1095.
- [7] Onoda H., Tanaka R. Synthesis of Cerium Phosphate White Pigments from Cerium Carbonate for Cosmetics. *J. Mater. Res. Technol.*, 2019, **8**, P. 5524–5528.
- [8] Achary S.N., Bevara S., Tyagi A.K. Recent Progress on Synthesis and Structural Aspects of Rare-Earth Phosphates. *Coord. Chem. Rev.*, 2017, **340**, P. 266–297.
- [9] Sato T., Li R., Sato C., Yin S. Synthesis and Photochemical Properties of Micaceous Cerium Phosphates. *Phosphorus Res. Bull.*, 2007, **21**, P. 44–47.
- [10] Sato T., Sato C., Yin S. Optimization of Hydrothermal Synthesis of Plate-Like Hydrated Cerium Phosphates and Their Photochemical Properties. *Phosphorus Res. Bull.*, 2008, **22**, P. 17–21.
- [11] Sato T., Yin S. Morphology Control of Cerium Phosphates for UV-Shielding Application. *Phosphorus Res. Bull.*, 2010, **24**, P. 43–48.
- [12] Kozlova T.O., Popov A.L., Kolesnik I. V., Kolmanovich D.D., Baranchikov A.E., Shcherbakov A.B., Ivanov V.K. Amorphous and Crystalline Cerium(IV) Phosphates: Biocompatible ROS-Scavenging Sunscreens. *J. Mater. Chem. B*, 2022, **10**, P. 1775–1785.
- [13] Nazaraly M., Quarton M., Wallez G., Chanéac C., Ribot F., Jolivet J.P. $\text{Ce}(\text{H}_2\text{O})(\text{PO}_4)_{3/2}(\text{H}_3\text{O})_{1/2}(\text{H}_2\text{O})_{1/2}$, a Second Entry in the Structural Chemistry of Cerium(IV) Phosphates. *Solid State Sci.*, 2007, **9**, P. 672–677.
- [14] Nazaraly M., Chanéac C., Ribot F., Wallez G., Quarton M., Jolivet J.P. A New Story in the Structural Chemistry of Cerium(IV) Phosphate. *J. Phys. Chem. Solids*, 2007, **68**, P. 795–798.

- [15] Nazaraly M., Wallez G., Chanéac C., Tronc E., Ribot F., Quarton M., Jolivet J.P. Synthesis and Characterization of $\text{CeIV}(\text{PO}_4)(\text{HPO}_4)_{0.5}(\text{H}_2\text{O})_{0.5}$. *J. Phys. Chem. Solids*, 2006, **67**, P. 1075–1078.
- [16] Brandel V., Clavier N., Dacheux N. Synthesis and Characterization of Uranium (IV) Phosphate-Hydrogenphosphate Hydrate and Cerium (IV) Phosphate-Hydrogenphosphate Hydrate. *J. Solid State Chem.*, 2005, **178**, P. 1054–1063.
- [17] Shekunova T.O., Istomin S.Y., Mironov A. V., Baranchikov A.E., Yapryntsev A.D., Galstyan A.A., Simonenko N.P., Gippius A.A., Zhurenko S.V., Shatalova T.B., Skogareva L.S., Ivanov V.K. Crystallization Pathways of Cerium(IV) Phosphates Under Hydrothermal Conditions: A Search for New Phases with a Tunnel Structure. *Eur. J. Inorg. Chem.*, 2019, **2019**, P. 3242–3248.
- [18] Kozlova T.O., Mironov A.V., Istomin S.Y., Birichevskaya K.V., Gippius A.A., Zhurenko S.V., Shatalova T.B., Baranchikov A.E., Ivanov V.K. Meet the Cerium(IV) Phosphate Sisters: $\text{Ce}^{\text{IV}}(\text{OH})\text{PO}_4$ and $\text{Ce}_2^{\text{IV}}\text{O}(\text{PO}_4)_2$. *Chem. – A Eur. J.*, 2020, **26**, P. 12188–12193.
- [19] Kozlova T.O., Vasilyeva D.N., Kozlov D.A., Teplonogova M.A., Baranchikov A.E., Simonenko N.P., Ivanov V.K. Synthesis and Thermal Behavior of $\text{KCe}_2(\text{PO}_4)_3$, a New Full-Member in the $\text{A}^{\text{IV}}\text{M}_2^{\text{IV}}(\text{PO}_4)_3$ Family. *Nanosyst. Phys. Chem. Math.*, 2023, **14**, P. 112–119.
- [20] Serpone N., Dondi D., Albini A. Inorganic and Organic UV Filters: Their Role and Efficacy in Sunscreens and Suncare Products. *Inorganica Chim. Acta*, 2007, **360**, P. 794–802.
- [21] Ngoc T., Moon C., Park L. Recent Trends of Sunscreen Cosmetic: An Update Review. *Cosmetics*, 2019, **6**, 64.
- [22] Geoffrey K., Mwangi A.N., Maru S.M. Sunscreen Products: Rationale for Use, Formulation Development and Regulatory Considerations. *Saudi Pharm. J.*, 2019, **27**, P. 1009–1018.
- [23] Tronev I.V., Sheichenko E.D., Razvorotneva L.S., Trufanova E.A., Minakova P.V., Kozlova T.O., Baranchikov A.E., Ivanov V.K. Microwave-Assisted Hydrothermal Synthesis of Ceric-Ammonium Phosphates $(\text{NH}_4)_2\text{Ce}(\text{PO}_4)_2 \cdot \text{H}_2\text{O}$ and $\text{NH}_4\text{Ce}_2(\text{PO}_4)_3$. *Russ. J. Inorg. Chem.*, 2023, **68**, P. 263–269.
- [24] Yapryntsev A.D., Baranchikov A.E., Ivanov V.K., Tret'yakov Y.D. Chromium(III) Oxyhydroxide Synthesis under Intense Sonication. *Dokl. Chem.*, 2012, **446**, P. 180–182.
- [25] Yapryntsev A.D., Baranchikov A.E., Gubanov N.N., Ivanov V.K., Tret'yakov Y.D. Synthesis of Nanocrystalline ZrO_2 with Tailored Phase Composition and Microstructure under High-Power Sonication. *Inorg. Mater.*, 2012, **48**, P. 494–499.
- [26] Yang G., Lin W., Lai H., Tong J., Lei J., Yuan M., Zhang Y., Cui C. Understanding the Relationship between Particle Size and Ultrasonic Treatment during the Synthesis of Metal Nanoparticles. *Ultrason. Sonochem.*, 2021, **73**, 105497.
- [27] Kozlova T.O., Baranchikov A.E., Birichevskaya K.V., Kozlov D.A., Simonenko N.P., Gavrikov A.V., Teplonogova M.A., Ivanov V.K. On the Thermal Decomposition of Cerium(IV) Hydrogen Phosphate $\text{Ce}(\text{PO}_4)(\text{HPO}_4)_{0.5}(\text{H}_2\text{O})_{0.5}$. *Russ. J. Inorg. Chem.*, 2021, **66**, P. 1624–1632.
- [28] Baranchikov A.E., Polezhaeva O.S., Ivanov V.K., Tret'yakov Y.D. Lattice Expansion and Oxygen Non-Stoichiometry of Nanocrystalline Ceria. *CrystEngComm*, 2010, **12**, P. 3531–3533.
- [29] Shekunova T.O., Baranchikov A.E., Ivanova O.S., Skogareva L.S., Simonenko N.P., Karavanova Y.A., Lebedev V.A., Borilo L.P., Ivanov V.K. Ceric Phosphate Gels: Synthesis, Thermal Decomposition and Hydrothermal Crystallization Paths. *J. Non. Cryst. Solids*, 2016, **447**, P. 183–189.
- [30] Kozlova T.O., Vasil'eva D.N., Kozlov D.A., Teplonogova M.A., Birichevskaya K.V., Baranchikov A.E., Gavrikov A.V., Ivanov V.K. On the Chemical Stability of $\text{Ce}^{\text{IV}}(\text{PO}_4)(\text{HPO}_4)_{0.5}(\text{H}_2\text{O})_{0.5}$ in Alkaline Media. *Russ. J. Inorg. Chem.*, 2022, **67**, P. 1901–1907.
- [31] Skogareva L.S., Shekunova T.O., Baranchikov A.E., Yapryntsev A.D., Sadovnikov A.A., Ryumin M.A., Minaeva N.A., Ivanov V.K. Synthesis of Cerium Orthophosphates with Monazite and Rhabdophane Structure from Phosphoric Acid Solutions in the Presence of Hydrogen Peroxide. *Russ. J. Inorg. Chem.*, 2016, **61**, P. 1219–1224.
- [32] Clavier N., Mesbah A., Szenknect S., Dacheux N. Monazite, Rhabdophane, Xenotime & Churchite: Vibrational Spectroscopy of Gadolinium Phosphate Polymorphs. *Spectrochim. Acta – Part A Mol. Biomol. Spectrosc.*, 2018, **205**, P. 85–94.
- [33] Petit S., Righi D., Madejová J. Infrared Spectroscopy of NH_4^+ -Bearing and Saturated Clay Minerals: A Review of the Study of Layer Charge. *Appl. Clay Sci.*, 2006, **34**, P. 22–30.
- [34] Petit S., Righi D., Madejová J., Decarreau A. Interpretation of the Infrared NH_4^+ Spectrum of the NH_4^+ -Clays: Application to the Evaluation of the Layer Charge. *Clay Miner.*, 1999, **34**, P. 543–549.
- [35] Klopogge J.T., Broekmans M., Duong L.V., Martens W.N., Hickey L., Frost R.L. Low Temperature Synthesis and Characterisation of Lecontite, $(\text{NH}_4)\text{Na}(\text{SO}_4)_2 \cdot \text{H}_2\text{O}$. *J. Mater. Sci.*, 2006, **41**, P. 3535–3539.
- [36] Kopitsa G.P., Baranchikov A.E., Ivanova O.S., Yapryntsev A.D., Grigoriev S. V., Pranzas P.K., Ivanov V.K. Effect of High Intensity Ultrasound on the Mesostructure of Hydrated Zirconia. *J. Phys. Conf. Ser.*, 2012, **340**, 012057.
- [37] Ivanov V.K., Kopitsa G.P., Sharikov F.Y., Baranchikov A.Y., Shaporev A.S., Grigoriev S.V., Pranzas P.K. Ultrasound-Induced Changes in Mesostructure of Amorphous Iron (III) Hydroxide Xerogels: A Small-Angle Neutron Scattering Study. *Phys. Rev. B*, 2010, **81**, 174201.
- [38] Kuznetsova V.A., Almjasheva O.V., Gusarov V.V. Influence of Microwave and Ultrasonic Treatment on the Formation of CoFe_2O_4 under Hydrothermal Conditions. *Glas. Phys. Chem.*, 2009, **35**, P. 205–209.
- [39] Rezaei P., Rezaei M., Meshkani F. Ultrasound-Assisted Hydrothermal Method for the Preparation of the $\text{M-Fe}_2\text{O}_3 \cdot \text{CuO}$ (M: Mn, Ag, Co) Mixed Oxides Nanocatalysts for Low-Temperature CO Oxidation. *Ultrason. Sonochem.*, 2019, **57**, P. 212–222.
- [40] Chorghand M., Haghighi M., Saedy S., Aghamohammadi S. Efficient Hydrothermal Synthesis of Nanostructured SAPO-34 Using Ultrasound Energy: Physicochemical Characterization and Catalytic Performance toward Methanol Conversion to Light Olefins. *Adv. Powder Technol.*, 2014, **25**, P. 1728–1736.
- [41] Kolesnik I.V., Shcherbakov A.B., Kozlova T.O., Kozlov D.A., Ivanov V.K. Comparative Analysis of Sun Protection Characteristics of Nanocrystalline Cerium Dioxide. *Russ. J. Inorg. Chem.*, 2020, **65**, P. 960–966.
- [42] Goh E.G., Xu X., McCormick P.G. Effect of Particle Size on the UV Absorbance of Zinc Oxide Nanoparticles. *Scr. Mater.*, 2014, **78–79**, P. 49–52.
- [43] Shi W., Lin Y., Zhang S., Tian R., Liang R., Wei M., Evans D.G., Duan X. Study on UV-Shielding Mechanism of Layered Double Hydroxide Materials. *Phys. Chem. Chem. Phys.*, 2013, **15**, 18217.
- [44] Kim J.H., Choi J., Choi S., Kim W., Lee S. Study on the Dependence of Sun Protection Factor on Particle Size Distribution of Mica Using Gravitational Field-Flow Fractionation. *Bull. Korean Chem. Soc.*, 2020, **41**, P. 66–72.
- [45] Silva M.R.F., Alves M.F.R.P., Cunha J.P.G.Q., Costa J.L., Silva C.A., Fernandes M.H.V., Vilarinho P.M., Ferreira P. Nanostructured Transparent Solutions for UV-Shielding: Recent Developments and Future Challenges. *Mater. Today Phys.*, 2023, **35**, 101131.

Information about the authors:

Taisiya O. Kozlova – Kurnakov Institute of General and Inorganic Chemistry of the Russian Academy of Sciences, Leninsky prospect, 31, Moscow, 119991, Russia; ORCID 0000-0002-9757-9148; taisia.shekunova@yandex.ru

Ekaterina D. Sheichenko – Kurnakov Institute of General and Inorganic Chemistry of the Russian Academy of Sciences, Leninsky prospect, 31, Moscow, 119991, Russia; National Research University Higher School of Economics, Moscow, Myasnitskaya str., 20, 101000, Russia; ORCID 0000-0003-3485-1842; kseterina@yandex.ru

Darya N. Vasilyeva – Kurnakov Institute of General and Inorganic Chemistry of the Russian Academy of Sciences, Leninsky prospect, 31, Moscow, 119991, Russia; National Research University Higher School of Economics, Moscow, Myasnitskaya str., 20, 101000, Russia; ORCID 0009-0004-3560-4178; dnvasilyeva_1@edu.hse.ru

Daniil A. Kozlov – Kurnakov Institute of General and Inorganic Chemistry of the Russian Academy of Sciences, Leninsky prospect, 31, Moscow, 119991, Russia; ORCID 0000-0003-0620-8016; kozlov@inorg.chem.msu.ru

Irina V. Kolesnik – Kurnakov Institute of General and Inorganic Chemistry of the Russian Academy of Sciences, Leninsky prospect, 31, Moscow, 119991, Russia; Lomonosov Moscow State University, Leninskie Gory 1, Moscow, 119991, Russia; ORCID 0000-0002-1411-6691; kolesnik.iv@gmail.com

Ilya V. Tronev – Kurnakov Institute of General and Inorganic Chemistry of the Russian Academy of Sciences, Leninsky prospect, 31, Moscow, 119991, Russia; National Research University Higher School of Economics, Moscow, Myasnitskaya str., 20, 101000, Russia; ORCID 0000-0002-0718-1911; ivtronev@edu.hse.ru

Maria A. Teplonogova – Kurnakov Institute of General and Inorganic Chemistry of the Russian Academy of Sciences, Leninsky prospect, 31, Moscow, 119991, Russia; ORCID 0000-0002-4820-8498; m.teplonogova@gmail.com

Alexander E. Baranchikov – Kurnakov Institute of General and Inorganic Chemistry of the Russian Academy of Sciences, Leninsky prospect, 31, Moscow, 119991, Russia; ORCID 0000-0002-2378-7446; a.baranchikov@yandex.ru

Vladimir K. Ivanov – Kurnakov Institute of General and Inorganic Chemistry of the Russian Academy of Sciences, Leninsky prospect, 31, Moscow, 119991, Russia; ORCID 0000-0003-2343-2140; van@igic.ras.ru

Conflict of interest: the authors declare no conflict of interest.